

Kinetic process of the phase separation in the alloy $\text{Ni}_3\text{Al}_{0.52}\text{V}_{0.48}$ Makoto Tanimura,¹ Akihiko Hirata,^{2,†} and Yasumasa Koyama²¹Research Department, NISSAN ARC, LTD., Yokosuka, Kanagawa 237-0061, Japan²Kagami Memorial Laboratory for Materials Science and Technology and Department of Materials Science and Engineering, Waseda University, Shinjuku, Tokyo 169-8555, Japan

(Received 12 November 2003; revised manuscript received 23 March 2004; published 22 September 2004)

In the $\text{Ni}_3\text{Al}_{0.52}\text{V}_{0.48}$ alloy, D0_{22} precipitation in the supersaturated L1_2 matrix has been found to stagnate due to the occurrence of the $\text{L1}_2 \rightarrow \text{L1}_2 + \text{D0}_{22} \rightarrow \text{L1}_2$ structural change in an isothermal process. In this paper, we experimentally show the variation of the L1_2 and D0_{22} chemical compositions during the structural change. Our results reveal that the transient D0_{22} formation accompanies a large concentration fluctuation, while the final L1_2 composition reverts back to the initial L1_2 one. It is also found that the average V content of the D0_{22} regions decreases together with the change in the $\text{L1}_2/\text{D0}_{22}$ habit planes from the $\{100\}$ to $\{110\}$ ones. These experimental results are indicative of the suppression of atomic diffusion and subsequent redistribution of Al and V in the L1_2 matrix, resulting in D0_{22} annihilation. It is proposed that jump site selectivity and cooperative atomic migration in the L1_2 structure are important factors in the suppression of atomic diffusion. Because the appearance of these factors correlates well with the vacancy concentration of the L1_2 matrix, it is concluded that the stagnation of D0_{22} precipitation represents one kinetic process under the present thermodynamic path.

DOI: 10.1103/PhysRevB.70.094111

PACS number(s): 64.75.+g, 05.70.-a, 66.30.-h, 82.60.Nh

I. INTRODUCTION

Phase separation in the form of precipitation or spinodal decomposition is one well-known phenomenon in alloys. Generally, a supersaturated solid solution undergoes phase separation under a given thermodynamic condition, e.g., while the alloy is kept at a constant temperature and pressure. The basic principle of phase separation is a minimization of the free energy in the system, ultimately resulting in an energy-minimum equilibrium state. In statistical thermodynamics, such an equilibrium state is defined on the basis of the ensemble average of microscopic states. On the other hand, phase separation is an irreversible relaxation phenomenon controlled by atomic diffusion, the kinetics of which is normally described on the basis of nonequilibrium thermodynamics. In the theoretical framework, the kinetics can be understood very well when the temporal development of the microscopic states in the system results in the attainment of the equilibrium state. However, if the time-developed state does not correspond correctly with the equilibrium state, it poses a major issue for statistical physics.

Atomic diffusion is subject to certain limits. For example, an atom at a site cannot jump to adjacent sites that are already occupied by other atoms. We can easily imagine that such “diffusion blocking” influences (to a greater or lesser extent) the kinetics of the phenomena controlled by atomic diffusion. Interestingly enough, Sato *et al.* have theoretically suggested that, because the blocking effect plays a crucial role in the time correlation of the diffusion flow, the time average (not the ensemble average) has to be used in evaluating observable quantities such as the correlation factor in the diffusion process.¹⁻⁴ This suggestion directly raises the issue that the relaxation process always faces. In order to obtain a better understanding of this issue, the phase separation of alloys having substitution-type ordered structures is one example that can be considered. This is because the atomic diffusion in ordered structures essentially includes the

selectivity of the jump sites, i.e., a more severe blocking effect in comparison with that in disordered structures.

In this study, we focus on D0_{22} precipitation in the supersaturated L1_2 matrix of pseudobinary $\text{Ni}_3\text{Al}_{1-x}\text{V}_x$ alloys. According to the phase diagram of the alloy system,⁵ as shown in Fig. 1, the $\text{Ni}_3\text{Al}_{0.2}\text{V}_{0.8}$ alloy undergoes the $\text{fcc} \rightarrow \text{L1}_2(\text{Ni}_3\text{V}) + \text{D0}_{22}(\text{Ni}_3\text{Al})$ eutectoid reaction at 1281 K. It should be mentioned here that the D0_{22} and L1_2 structures are A_3B -type ordered ones based on the fcc lattice. Because ice-water quenching from the fcc region cannot suppress the L1_2 ordering in the $\text{Ni}_3\text{Al}_{0.6-0.4}\text{V}_{0.4-0.6}$ alloys, the quenched

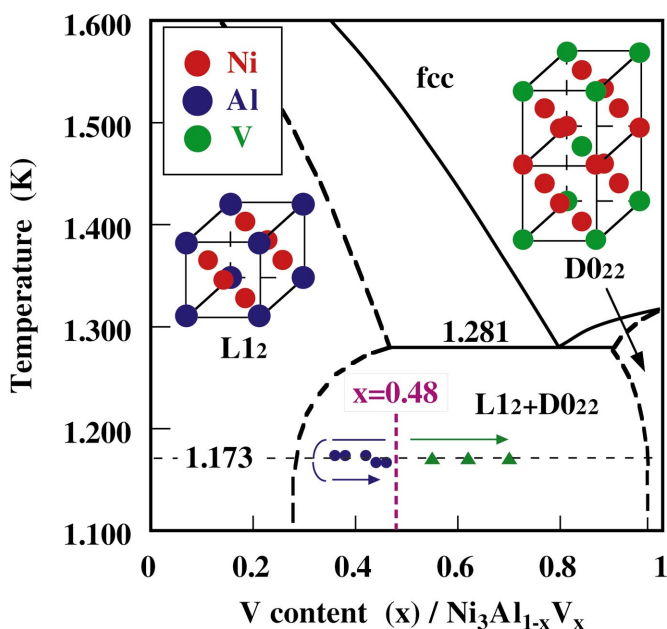


FIG. 1. (Color) Phase diagram of the pseudobinary $\text{Ni}_3\text{Al}_{1-x}\text{V}_x$ alloy system. Diagrams of the D0_{22} and the L1_2 structures and the measured V content are inserted.

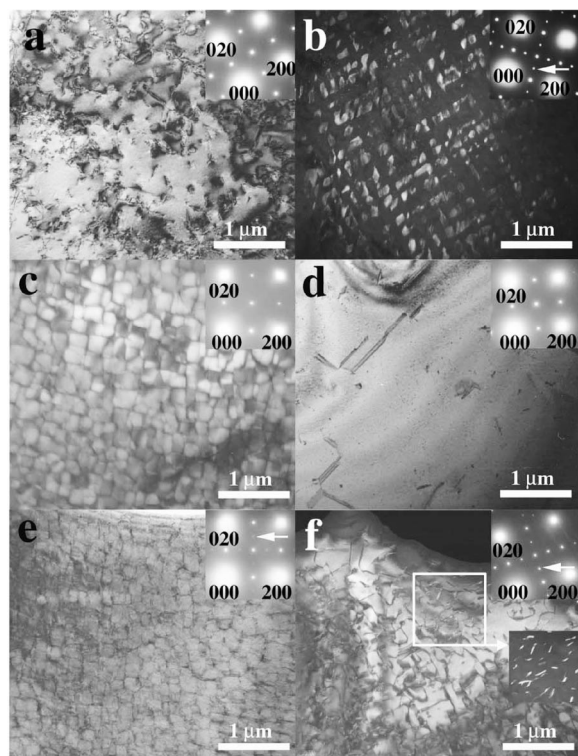


FIG. 2. Microstructures of the $\text{Ni}_3\text{Al}_{1-x}\text{V}_x$ alloys. (a) Electron diffraction pattern and bright field image obtained from the quenched $\text{Ni}_3\text{Al}_{0.60}\text{V}_{0.40}$ alloy. (b) Electron diffraction pattern and dark field image taken by using the $1/2\ 1\ 0$ spot obtained from the $\text{Ni}_3\text{Al}_{0.60}\text{V}_{0.40}$ alloy kept at 1173 K for 100 h. (c) Electron diffraction pattern and bright field image obtained from the quenched $\text{Ni}_3\text{Al}_{0.52}\text{V}_{0.48}$ alloy. (d) Electron diffraction pattern and bright field image obtained from the $\text{Ni}_3\text{Al}_{0.52}\text{V}_{0.48}$ alloy kept at 1173 K for 1000 h. (e) Electron diffraction pattern and bright field image obtained from the quenched $\text{Ni}_3\text{Al}_{0.45}\text{V}_{0.55}$ alloy. (f) Electron diffraction pattern and dark field image taken by using the $1\ 0\ 0$ spot obtained from the $\text{Ni}_3\text{Al}_{0.45}\text{V}_{0.55}$ alloy kept at 1173 K for 100 h. A dark-field image of the square region, which was taken by using the $1/2\ 1\ 0$ spot, is shown in the inset, where the bright-contrast regions correspond to the D0_{22} regions.

alloys basically consist of the supersaturated L1_2 single phase as a metastable state.^{6–8} Hence, keeping the quenched alloys at a temperature lower than 1281 K ought to promote D0_{22} precipitation in the L1_2 matrix, including the $\text{L1}_2 \rightarrow \text{D0}_{22}$ structural change, resulting in the formation of the $\text{L1}_2 + \text{D0}_{22}$ equilibrium state. Nevertheless, we observed that D0_{22} precipitation was suppressed in the $\text{Ni}_3\text{Al}_{0.52}\text{V}_{0.48}$ alloy due to the occurrence of the $\text{L1}_2 \rightarrow \text{L1}_2 + \text{D0}_{22} \rightarrow \text{L1}_2$ structural change even when the quenched alloy was kept at 1173 K for as long as 1000 h.⁹ It was clear that the final state obtained via the structural change was not the $\text{L1}_2 + \text{D0}_{22}$ equilibrium state. In order to understand the kinetics of this unique phenomenon, the changes in the chemical compositions during the structural change of the $\text{Ni}_3\text{Al}_{0.52}\text{V}_{0.48}$ alloy were examined by analytical electron microscopy. The physical cause of the suppression of the phase separation will be discussed here on the basis of the experimental results.

II. EXPERIMENTAL PROCEDURE

Ingots of the $\text{Ni}_3\text{Al}_{1-x}\text{V}_x$ alloys ($x=0.4–0.6$) were made by an Ar-arc melting technique and homogenized at the fcc region for 24 h. In reference to the phase diagram shown in Fig. 1, the ingots were homogenized at different temperatures, e.g., 1673 K for the $\text{Ni}_3\text{Al}_{0.60}\text{V}_{0.40}$ alloy and 1573 K for the $\text{Ni}_3\text{Al}_{0.52}\text{V}_{0.48}$ and $\text{Ni}_3\text{Al}_{0.45}\text{V}_{0.55}$ alloys, followed by ice-water quenching. Because all of the quenched ingots basically consisted of the L1_2 single phase, samples cut from each ingot were kept at 1173 K ($\text{L1}_2 + \text{D0}_{22}$ region) to induce D0_{22} precipitation in the L1_2 matrix. In order to examine the transitional states of the phase separation, the respective samples were kept at that temperature for 0.17 (10 min), 0.5, 1, 5, 10, 100, and 1000 h and then quenched in ice-water again.

Observation and analysis of the samples were carried out by using a TECNAI G² F20 scanning transmission electron microscope with an acceleration voltage of 200 keV. The electron incidence in both the observation and the analysis was basically parallel to one of the $\langle 001 \rangle$ directions (in this paper, for simplicity, all of the Miller's indices and the diffraction spots are denoted in terms of the fcc notation). This is because the interface between the L1_2 matrix and the D0_{22} precipitates was perpendicular to one of the $\{001\}$ planes. The microstructures were examined by taking bright- and dark-field images as well as electron diffraction patterns. Energy dispersive x-ray (EDX) mapping diagrams were obtained by scanning the samples with an electron probe about 1 nm in diameter and by using the characteristic x-ray of the V- $\text{K}\alpha$ line as well as the Ni- $\text{K}\alpha$ and Al- $\text{K}\alpha$ lines. A point analysis was also carried out to determine the compositions of the L1_2 matrix, the D0_{22} precipitates and the stacking faults that appeared in the respective samples. For quantification, we used the Ni- $\text{K}\alpha$, Al- $\text{K}\alpha$, and V- $\text{K}\alpha$ lines and obtained a measured value resolution of about $x = \pm 0.02$.

III. EXPERIMENTAL RESULTS

In order to present a total picture of the phase separation process, i.e., D0_{22} precipitation in the supersaturated L1_2 matrix, we will start with a simple description of the morphological changes that occur in the $\text{Ni}_3\text{Al}_{1-x}\text{V}_x$ ($x=0.4–0.6$) alloys while being kept at 1173 K. Figure 2(a) shows a typical bright-field image and an electron diffraction pattern obtained from the quenched $\text{Ni}_3\text{Al}_{0.60}\text{V}_{0.40}$ alloy. Because L1_2 ordered spots as well as fcc fundamental spots are detected (no D0_{22} ordered spots exist) in the diffraction pattern, the quenched alloy consists of the supersaturated L1_2 single state. In terms of its morphology, the L1_2 single state includes a lot of dislocations, as shown in the bright-field image. When the quenched alloy was kept at 1173 K, the D0_{22} regions nucleated at the dislocations and grew in the L1_2 matrix, although the details are not shown here. In a diffraction pattern obtained from a sample kept at 1173 K for 100 h, Fig. 2(b), the diffraction spots present at $1/2\ 1\ 0$ -type positions imply the existence of the D0_{22} regions. Actually, in the dark-field image taken by using a $1\ 1/2\ 0$ spot, one of the D0_{22} variants giving rise to the bright contrast can be

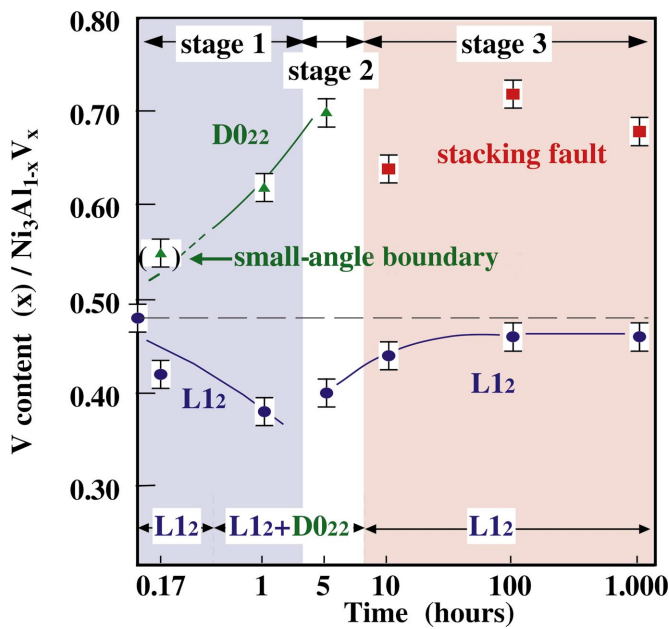


FIG. 3. (Color) V-content variation as a function of the time the $\text{Ni}_3\text{Al}_{0.52}\text{V}_{0.48}$ alloy was kept at 1173 K. The time of 0 h corresponds to the quenched sample. Each value is an average of 15 measured values.

observed. A crystallographic feature of the $\text{L1}_2/\text{D0}_{22}$ state is that the $\text{L1}_2/\text{D0}_{22}$ habit plane is the $\{110\}$ plane, as reported previously.^{7,8} These results clearly indicate that D0_{22} precipitation in the L1_2 matrix occurs in the alloy during the isothermal process. In case of the $\text{Ni}_3\text{Al}_{0.52}\text{V}_{0.48}$ alloy, however, D0_{22} precipitation is suppressed. As shown in the diffraction pattern and bright-field image in Fig. 2(c), the quenched alloy is in the L1_2 single state and includes a lot of small-angle tilt boundaries along one of the $\langle 100 \rangle$ directions. Even though the quenched alloy was kept at 1173 K for 1000 h, no D0_{22} regions can be observed and the state obtained is the L1_2 single one [see Fig. 2(d)]. In the case of the $\text{Ni}_3\text{Al}_{0.45}\text{V}_{0.55}$ alloy, the $\text{L1}_2+\text{D0}_{22}$ state also forms while the alloy is kept at 1173 K. Figure 2(e) shows a diffraction pattern and corresponding bright-field image obtained from the quenched alloy. The diffraction pattern is basically composed of the spots due to the L1_2 and fcc structures. An important feature of the pattern is that the ordered spots attributed to the D0_{22} structure are also detected at $1/2\ 1\ 0$ -type positions with very weak intensities. This implies that, in addition to the L1_2 ordering, the D0_{22} ordering occurs locally in the quenched alloy. In the corresponding bright-field image, the L1_2 state can be observed with a lot of small-angle tilt boundaries running mainly along one of the $\langle 100 \rangle$ directions. A detailed analysis by taken some dark-field images reveals that some boundaries adopt the D0_{22} configuration. A dark-field image taken by using a $1\ 0\ 0$ spot obtained from the alloy kept at 1173 K for 100 h is shown in Fig. 2(f). It is observed in this image that dark string-like regions exist in the L1_2 matrix with the bright contrast. The dark-field images taken by using $1/2\ 1\ 0$ -type spots, an example of which is shown in the inset in Fig. 2(f), indicate that a large portion of these regions corresponds to the D0_{22} precipitates. This

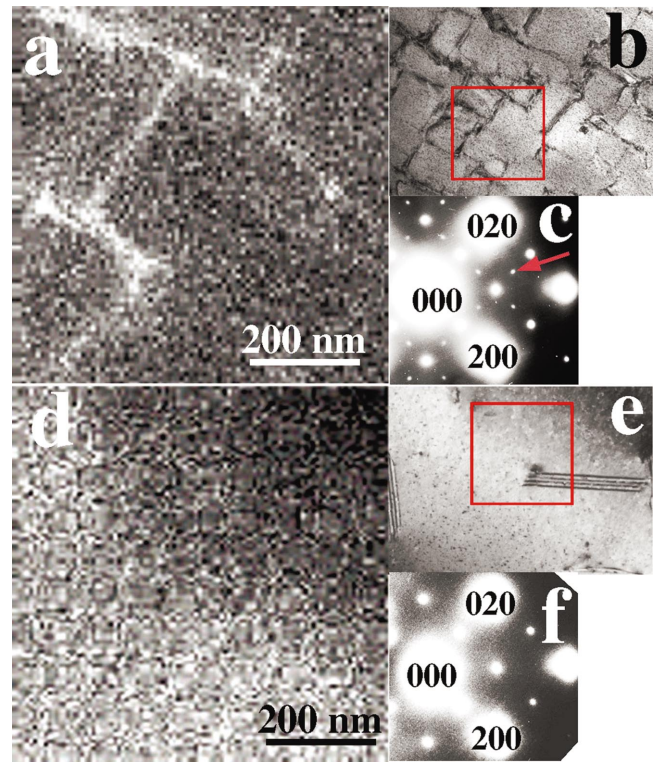


FIG. 4. (Color) Microstructures in stages 1 and 3 of the $\text{Ni}_3\text{Al}_{0.52}\text{V}_{0.48}$ alloy. (a) V-mapping diagram obtained from the red-square area in the image in (b). The bright-contrast region has a larger V content than the dark-contrast region. (b) Bright-field image obtained from a sample aged for 1 h. Intermittive D0_{22} regions with the dark contrast are present along the $\langle 100 \rangle$ directions in the L1_2 matrix with the bright contrast. (c) Electron diffraction pattern corresponding to the area shown in (a). (d) V-mapping diagram obtained from the red-square area in the image in (d). (e) Bright-field image obtained from a sample kept at 1173 K for 100 h. The fringe-contrast regions correspond to the $\{111\}$ stacking faults. (f) Electron diffraction pattern corresponding to the area shown in (d).

implies that the $\text{L1}_2/\text{D0}_{22}$ boundaries have a tendency to rotate from the $\{100\}$ to $\{110\}$ planes, with the result that a $\text{L1}_2+\text{D0}_{22}$ state having a maze pattern is formed in the alloy. Note that this tendency is well consistent with that of the $\text{Ni}_3\text{Al}_{0.60}\text{V}_{0.40}$ alloy. Eventually, the experimental results reveal that the suppression of D0_{22} precipitation takes place only in a limited composition range, i.e., $0.45 < x < 0.55$ of the $\text{Ni}_3\text{Al}_{1-x}\text{V}_x$ alloys examined in this work.

In order to understand the kinetics of the suppression of D0_{22} precipitation, we will focus here on the $\text{L1}_2 \rightarrow \text{L1}_2 + \text{D0}_{22} \rightarrow \text{L1}_2$ structural change occurring in the $\text{Ni}_3\text{Al}_{0.52}\text{V}_{0.48}$ alloy. On the basis of the change in the crystallographic and morphological features reported previously,⁹ we will show the variation in the chemical composition of both the D0_{22} precipitates and the L1_2 matrix that occurred while the temperature of the alloy was kept at 1173 K. Figure 3 shows the changes in the average V content of both the L1_2 matrix and the D0_{22} precipitates during the isothermal process. The data show that there are three stages in terms of the V-content variation. Stage 1 corresponds to the appearance of the D0_{22} regions, where the V content of the L1_2

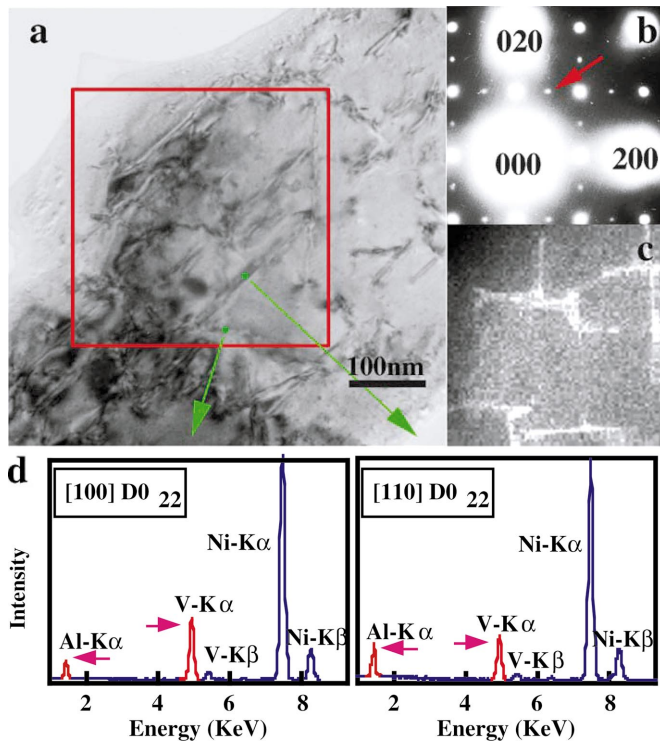


FIG. 5. (Color) Microstructures in stage 2 of the $\text{Ni}_3\text{Al}_{0.52}\text{V}_{0.48}$ alloy. (a) Bright-field image obtained from a sample kept at 1173 K for 5 h. Rotating D0_{22} regions are present in the L1_2 matrix. (b) Electron diffraction pattern corresponding to the area shown in the image. The pattern indicates that the D0_{22} regions still exist in the sample. (c) V-mapping diagram of the red-square area in the image. (d) EDX profiles obtained from the [100]- and [110]-oriented D0_{22} regions. The measured points are labeled in the image. The characteristic x-ray intensities of both profiles are normalized by using the Ni-K α lines.

matrix decreases to about 0.38, while that of the D0_{22} precipitates increases to about 0.70. These composition changes imply that the appearance of the D0_{22} regions is controlled by V diffusion. Once the $\text{L1}_2 + \text{D0}_{22}$ state is formed, the D0_{22} regions are annihilated when their V content reaches about 0.70 (see the changes in stage 2). An important feature of stage 2 is that there is a slight increase in the V content of the L1_2 matrix accompanying D0_{22} annihilation. In the subsequent stage 3 with a hold time of longer than 5 h, surprisingly, the V content of the L1_2 matrix slowly returns to about 0.45, which is close to the initial L1_2 composition. Because the stacking faults introduced on the {111} plane of the L1_2 structure have a large V content of 0.68 on average, this slight difference in the V content between the initial and final L1_2 matrices is attributed to the segregation of V at the faults. From these results, it is found that the appearance and subsequent annihilation of the D0_{22} regions accompanies a large and reversible-like variation of the V content in the L1_2 matrix. The V-content values obtained from the EDX analysis are plotted in the phase diagram shown in Fig. 1. As can be seen from the plots, it would appear that the alloy went back halfway to the L1_2 single state during the isothermal process.

The EDX analysis revealed that the turning point of the composition fluctuation was stage 2. Before going into any

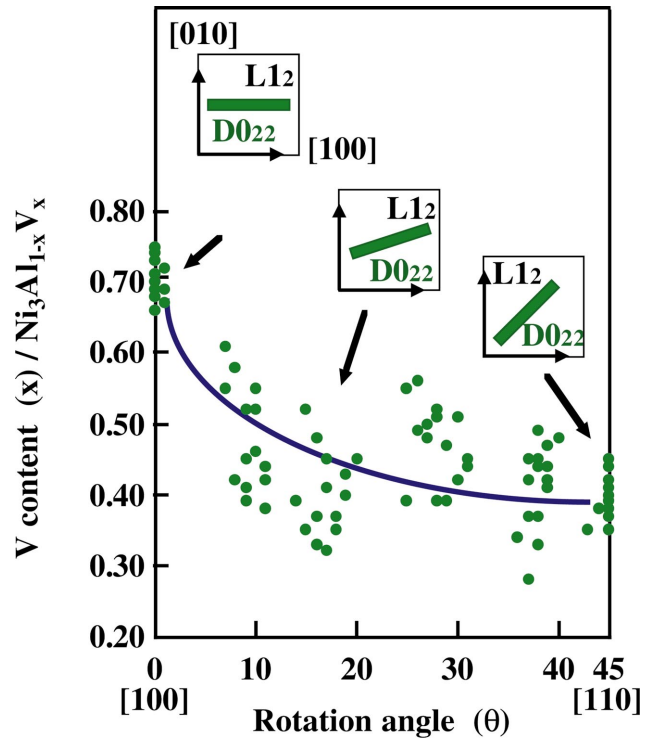


FIG. 6. (Color) V-content variation of the D0_{22} regions in terms of their rotation angles, obtained from a sample kept for 5 h. Schematic diagrams of the D0_{22} region rotation are inserted. The angle $\theta = 0^\circ$ corresponds to the [100] direction and the angle $\theta = 45^\circ$ to the [110] one of the L1_2 matrix.

further details of stage 2, the features of the V migration in stages 1 and 3 will be simply described. Initially, in stage 1, V concentrates on the small-angle tilt boundaries and the D0_{22} regions appear there when their V content increases to about 0.55. Figure 4(a) shows a V-mapping diagram obtained from a sample kept at 1173 K for 1 h, Fig. 4(b) a corresponding bright-field image, and Fig. 4(c) an electron diffraction pattern. The diffraction pattern confirms the appearance of the D0_{22} regions in the L1_2 matrix in the sample. The V-mapping diagram actually shows a larger V content in the D0_{22} regions than in the L1_2 matrix. On the other hand, the microstructure of the $\text{Ni}_3\text{Al}_{0.52}\text{V}_{0.48}$ alloy in stage 3 is the L1_2 single state including the {111} stacking faults. A typical V-mapping diagram obtained from a sample kept at 1173 K for 100 h is shown in Fig. 4(d), with a corresponding bright-field image, Fig. 4(e), and an electron diffraction pattern, Fig. 4(f). Note that the D0_{22} ordered spots located at $1/2$ 1 0-type positions disappear in the diffraction pattern. There is no evidence of V localization in the V-mapping diagram, indicating the uniform distribution of V in the {001} plane of the L1_2 structure. It should be noted here that V segregates at the stacking faults as shown in Fig. 3, which was confirmed in an EDX point analysis with the electron incidence parallel to the {111} plane.

Here we will give a detailed description of the features of the atomic migration in stage 2. The typical microstructure of a sample kept at 1173 K for 5 h is shown in a bright-field image in Fig. 5(a), together with an electron diffraction pattern, Fig. 5(b), a V-mapping diagram, Fig. 5(c), and the EDX

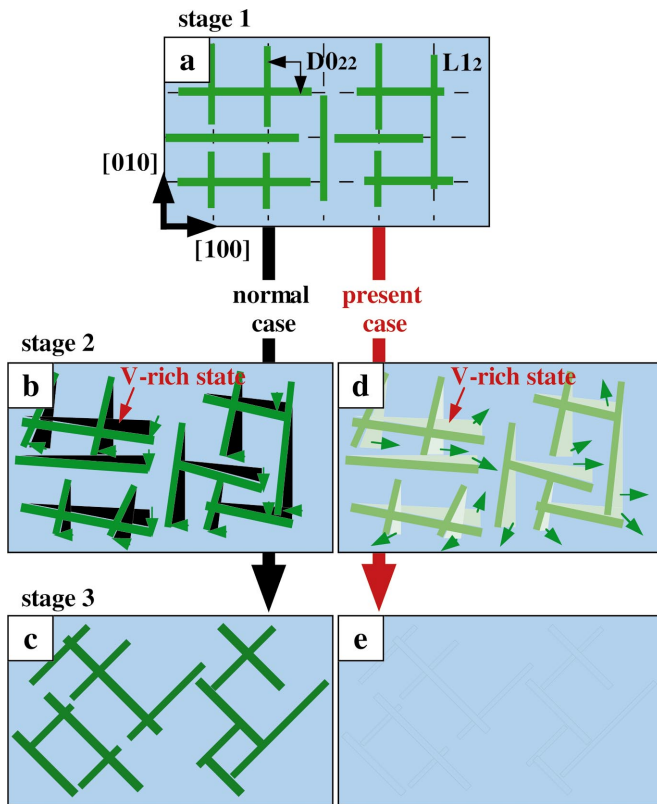


FIG. 7. (Color) Schematic diagram of the morphological evolution in the $D0_{22}$ precipitation (normal case) and $D0_{22}$ annihilation (present case) processes. (a) The morphology of stage 1. The $D0_{22}$ regions and the small-angle tilt boundaries are depicted by the green regions and the dashed lines, respectively. (b) and (c) The morphologies of stages 2 and 3 in the normal case. The V-rich $L1_2$ regions are denoted as the dotted regions. The $L1_2+D0_{22}$ maze pattern is finally formed with the change in the habit planes, followed by V migration. (d) and (e) The morphologies of stages 2 and 3 in the present case. The V-rich $L1_2$ regions are denoted as the light-green regions. $D0_{22}$ precipitation is suppressed due to the redistribution of V to the $L1_2$ matrix.

profiles, Fig. 5(d). The electron diffraction pattern indicates the coexistence of the $L1_2$ and $D0_{22}$ regions in this sample, and the band-like $D0_{22}$ regions oriented to the $\langle 100 \rangle$ and $\langle 110 \rangle$ directions in the $L1_2$ matrix are observed in the bright-field image. As described in previous papers,^{6,8} the misfit strain introduced in the $L1_2$ matrix due to the formation of the $D0_{22}$ regions causes the regions to rotate. Considering the crystallographic relation between the $D0_{22}$ and the $L1_2$ structures indicated by the electron diffraction pattern, the change in the habit planes from the $\{100\}$ to $\{110\}$ ones is essential for this rotation. The V-mapping diagram indicates a feature of deep interest; i.e., only the $\langle 100 \rangle$ -oriented $D0_{22}$ regions give rise to the bright contrast. Actually, the relative intensity of the V- $K\alpha$ line in the EDX profile obtained from the $\langle 110 \rangle$ -oriented $D0_{22}$ regions is smaller than that from the $\langle 100 \rangle$ -oriented regions (see the EDX spectra indicated by the arrows). This implies that the rotation causes a decrease in the V content of the $D0_{22}$ regions. In order to understand the details of this V-content depletion, we examined the change in the V content of the $D0_{22}$ regions with respect to their

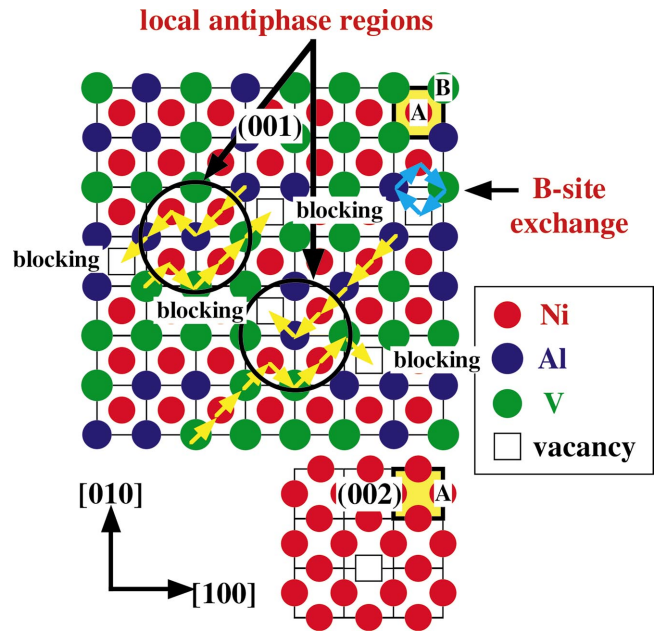


FIG. 8. (Color) Schematic diagram of the $L1_2$ configurations in the (001) and (002) planes. Examples of atomic migration are depicted in the diagram.

rotation. Figure 6 indicates the change in the V content (x) as a function of the rotation angle (θ) of the $D0_{22}$ regions from the $[100]$ direction. Schematic diagrams of the $D0_{22}$ region rotation are inserted in Fig. 6. We can see from Fig. 6 that, as the rotation angle increases, the average V content decreases from 0.70 (the average content of the $[100]$ -oriented $D0_{22}$ regions) to 0.40 (the average content of the $L1_2$ matrix) with a large degree of fluctuation. This indicates that the change in the habit planes gives rise to the V migration from the $D0_{22}$ regions to the $L1_2$ matrix. Note that the V content of the $L1_2$ matrix increases slightly in stage 2. The experimental results shown in Fig. 6 are thus direct evidence that the change in the habit planes acts as a trigger of the reversible-like V migration, resulting in $D0_{22}$ annihilation.

IV. DISCUSSION

Our results reveal that the transient $D0_{22}$ formation accompanies a large concentration fluctuation, whereas the final $L1_2$ composition returns back to the initial $L1_2$ one in the isothermal process. It is obvious that the final $L1_2$ state has lower free energy than the initial state due to the annihilation of a lot of small-angle tilt boundaries and the growth of the $L1_2$ grains. Thus, from a thermodynamic point of view, the final $L1_2$ state is obtained basically by $L1_2$ grain growth. However, the degree of the concentration fluctuation in the growth process indicates that the appearance and subsequent annihilation of the $D0_{22}$ regions originates from the long-range atomic diffusion, like a regular process of $D0_{22}$ precipitation, rather than from the short-range atomic rearrangement at the boundaries. Obviously, ordinal theoretical descriptions for the diffusion-controlled relaxation phenomena cannot explain this peculiar diffusion process. The origin of this peculiar phenomenon is discussed here on the basis of the experimental results.

Figure 7 shows schematic diagrams of the features of the morphological evolution in the isothermal process. In stage 1, as has been reported, the $D0_{22}$ regions appear at one of the $\langle 100 \rangle$ small-angle tilt boundaries with a V content of about $x=0.70$ [see Fig. 7(a)]. When the $L1_2/D0_{22}$ habit plane begins to change from the $\{100\}$ to the $\{110\}$ plane, the V content of the $D0_{22}$ regions decreases to about $x=0.40$ (stage 2, see Fig. 6). Because of this decrease, the $L1_2$ matrix in the vicinity of the $D0_{22}$ regions should be in a V-rich state. Here we consider two possible types of V behavior in the V-rich regions. One is the normal case depicted in Figs. 7(b) and 7(c), and the other is the present case as shown in Figs. 7(d) and 7(e). The V-rich regions are indicated by the red arrows in Figs. 7(b) and 7(d), respectively. Normally, V in the V-rich regions should follow the change in the habit planes, as shown by the green arrows in Fig. 7(b), enabling the phase separation to proceed, and resulting in the formation of the $L1_2+D0_{22}$ maze (or a checkerboard-like) pattern with the $\{110\}$ habit planes [see Fig. 7(c)]. For instance, the $L1_2+D0_{22}$ maze pattern obtained in the $Ni_3Al_{0.45}V_{0.55}$ alloy is considered to be in the midst of this process. In the present case, however, the change in the habit planes is not followed by V migration, as indicated in Fig. 6. As a result, the $D0_{22}$ regions are annihilated due to the redistribution of V into the $L1_2$ matrix, as schematically depicted by the green arrows in Fig. 7(d), and the $L1_2$ single state, including lattice defects, is formed in stage 3 [see Fig. 7(e)]. This scenario implies that the V behavior in the V-rich $L1_2$ matrix holds the key to the state toward which the system heads in the isothermal process.

We will describe the origin of the suppression of V diffusion in the V-rich $L1_2$ matrix that occurred in the present case. Because the crystallographic orientation of the fcc lattice is maintained during the structural change, a change in the atomic configuration on the fcc lattice is essential for suppression of V diffusion to occur. It should be mentioned here that the $L1_2 \rightarrow D0_{22}$ structural change is achieved by the antiphase $\langle 110 \rangle$ -atomic displacement in every other $\{001\}$ plane (refer to the structural diagrams in Fig. 1). Figure 8 shows a schematic diagram of the $L1_2$ atomic configuration on the (001) and (002) planes of the V-rich $L1_2$ state. The A and B sites correspond to the face-centered and edge sites of the fcc lattice, respectively, and the yellowed cell corresponds to the unit $L1_2$ configuration. In the diagram, Al and V are randomly located on the B sites, while Ni and vacancies exist on the A sites (for simplicity, the antisite defects are ignored). This is because V preferentially occupies the Al (B) site,¹⁰⁻¹² whereas the vacancies are preferentially located at the Ni (A) sites^{13,14} of the Ni_3Al alloy. An important feature of the atomic migration is that a B-site atom cannot jump directly to another B site because the B sites are not adjacent to each other. Therefore, in order for one B-site atom to replace another atom, the atom must jump by using an A-site vacancy on the (001) and /or (002) planes. One possible model of such jumping is depicted by the blue arrows. This implies that an exchange of B-site atoms without disturbing the $L1_2$ configuration requires at least two jumps, e.g., $B \rightarrow A \rightarrow B$ jumps along the $\langle 110 \rangle$ directions together with the cooperative jump of the A-site atom. Such a se-

quence of jumps is a fundamental process of atomic migration in the $L1_2$ configuration, but the small number of vacant B sites means there is a severe limitation on available jump sites.

Here we propose the directional migration of atoms, denoted by the yellow arrows, as one possible model that can occur in the $L1_2$ matrix. In principle, V and Al must migrate in opposite directions to follow the change in the habit planes. As is easily understood, however, this migration does not use the A-site vacancies effectively. Thus, V or Al at an A site cannot undergo an $A \rightarrow B$ jump when other atoms have occupied all of the adjacent B sites. As a result, Al and V cannot diffuse any more and local antiphase regions are formed, as indicated by the thick circles. When such blocking of atomic diffusion appears at random places on all of the (001) planes, phase separation stagnates, resulting in the formation of the $L1_2$ antiphase domains. Although the assist of the strain field must also be taken into account, diffusion blocking is essential to trigger the formation of the $L1_2$ single state, including a lot of antiphase boundaries at stage 2, as obtained in the alloys kept at 1173 K for 10 h.⁹

The uniform redistribution of V and Al in the $L1_2$ single state in stage 3 is a response of the atoms when very little directional migration occurs due to the blocking effect. One conceivable cause of the redistribution is an increase in configuration entropy. It should be noted here that this atomic behavior is quite opposite to that in stage 1. This clearly implies that the observable quantities such as the diffusion coefficient and the correlation factor of the diffusion flow do not have fixed values throughout the isothermal process. On the basis of the above-mentioned mechanism, the configuration of atoms and vacancies in the $L1_2$ state at any given instant in time dominates the atomic behavior at next instant due to the blocking effect. That is, the variability of the observable quantities is derived from time averaging (not ensemble averaging) of the microscopic state developed with time, as has been suggested theoretically.¹⁻⁴ The variation in the chemical composition shown in Fig. 3 is, therefore, experimental evidence that time averaging must be taken into account to estimate the observable quantities of atomic diffusion.

The appearance of the blocking effect should correlate well with the vacancy concentration. It is natural to assume that atomic jumps can occur more easily as the vacancy concentration of the initial $L1_2$ state increases. Thus, the difference in the thermodynamic paths substantially influences the kinetics of the phase separation in terms of the introduction of vacancies. Actually, the microstructures of the initial $L1_2$ states of the $Ni_3Al_{0.60}V_{0.40}$, $Ni_3Al_{0.52}V_{0.48}$, and $Ni_3Al_{0.45}V_{0.55}$ alloys are quite varied, and are formed under different thermodynamic conditions, e.g., homogenization temperature and deviation of the chemical compositions of the $L1_2$ single states from the stoichiometric (Ni_3Al) one. These conditions vary the vacancy concentration of the initial $L1_2$ states and, that variation also changes the way in which atomic migration occurs in the process of phase separation. Therefore, the final pattern can bifurcate in the phase separation of alloys, i.e., the time-developed state does not always correspond to

the equilibrium state when a strong blocking effect occurs in the diffusion process. It is concluded that the stagnation of phase separation in the $\text{Ni}_3\text{Al}_{0.52}\text{V}_{0.48}$ alloy corresponds to one kinetic process under the present thermodynamic path.

ACKNOWLEDGMENT

One of the authors (M. T.) acknowledges the technical support of K. Inoke, FEI Company Japan Ltd.

*Author to whom correspondence should be addressed. Electronic mail: tanimura@nissan-arc.co.jp

†Present address: The Institute of Scientific and Industrial Research, Osaka University, Ibaraki, Osaka 567-0047, Japan.

¹H. Sato and R. Kikuchi, *Phys. Rev. B* **28**, 648 (1983).

²H. Sato, T. Ishikawa, and R. Kikuchi, *J. Phys. Chem. Solids* **46**, 1361 (1985).

³H. Sato, K. Wada, A. Suzuki, and S. A. Akbar, *Solid State Ionics* **18–19**, 178 (1986).

⁴H. Sato and A. Datta, *Solid State Ionics* **72**, 19 (1994).

⁵Y. Hong, Y. Mishima, and T. Suzuki, *Mater. Res. Soc. Symp. Proc.* **133**, 429 (1989).

⁶L. A. Bendersky, F. S. Biancaniello, and M. E. Williams, in *Solid-solid Phase Transformations*, edited by W. C. Johnson, J. M. Howe, D. E. Laughlin, and W. A. Soffa (TMS,PA, 1994),

pp. 899–904.

⁷M. Takeyama and M. Kikuchi, *Intermetallics* **6**, 573 (1998).

⁸R. Poduri and L.-Q. Chen, *Acta Mater.* **46**, 1719 (1998).

⁹M. Tanimura, M. Kikuchi, and Y. Koyama, *J. Phys.: Condens. Matter* **14**, 7053 (2002).

¹⁰M. Morinaga, N. Yukawa, and H. Adachi, *J. Phys. Soc. Jpn.* **53**, 653 (1984).

¹¹J.-H. Xu, T. Oguchi, and A. J. Freeman, *Phys. Rev. B* **36**, 4186 (1987).

¹²W. Lin, J.-H. Xu, and A. J. Freeman, *Phys. Rev. B* **45**, 10863 (1992).

¹³S. M. Kim, *J. Mater. Res.* **6**, 1455 (1991).

¹⁴H. Numakura, T. Ikeda, M. Koiwa, and A. Almazouzi, *Philos. Mag. A* **77**, 887 (1998).